Meteorol. Atmos. Phys. 41, 191–211 (1989)

Meteorology and Atmospheric Physics

551.513.1

Department of Marine, Earth and Atmospheric Sciences, North Carolina State University, Raleigh, North Carolina, U.S.A.

A Study of the Seasonal Migration of ITCZ and the Quasi-Periodic Oscillations in a Simple Monsoon System Using an Energy Balance Model

K. Alapati and **S. Raman**

With 22 Figures

Received January 10, 1989
Revised June 8, 1989

Summary

A zonally averaged global energy balance model with feedback mechanisms was constructed to simulate (i) the poleward limits of ITCZ over the continent and over the ocean and (ii) a simple monsoon system as a result of differential heating between the continent and the ocean. Three numerical experiments were performed with lower boundary as (1) global continent, (2) global ocean and (3) continent-ocean, with freezing latitudes near the poles. Over the continent, midlatitude deserts were found and the ITCZ migrates 25° north and south with seasons. Over a global swamp ocean results do not show migration of ITCZ with time but once the ocean currents are introduced the ITCZ migrates 5° north and south with seasons. It was found that the seasonal migration of ITCZ strongly depends on the meridional distribution of the surface temperature. It was also found that continent influences the location of the oceanic ITCZ. In the tropics northward progression of quasi-periodic oscillations called "events" are found during the pre- and post-monsoon periods with a period of 8 to 15 days. This result is consistent with the observed quasi-periodic oscillations in the tropical region. Northward propagation of the surface temperature perturbation appears to cause changes in the sensible heat flux which in turn causes perturbations in vertical velocity and latent heat flux fields.

List of Symbols

Let ψ be some variable. Then the convention used is

$\bar{\psi}$	vertical average
ψ_0	zonal average
$\bar{\psi}_0$	vertical mean of the zonal average
ψ_{0s}	zonal average at the surface
$\psi_{0\alpha}$	zonal average at 500 mb level

We now define the various symbols used in the model.

φ	latitude
Φ	rate of atmospheric heating due to convective cloud formation (K/sec)
ω	dp/dt (N/m^2/sec)
ρ	density
θ	potential temperature (K)
Ω	rate of rotation of the earth (rad/sec)
ξ	empirical constant
ε	humidity mixing ratio
ε^*	saturated humidity mixing ratio
χ	opacity of the atmosphere
γ_1, γ_2	factors for downward and upward effective black body long wave radiation from the atmosphere
σ	Stefan-Boltzmann constant
Γ	emissivity of the surface
θ_D	subsurface temperature (K)
a	specific volume
τ_{0xs}, τ_{0ys}	eastward and northward components of surface frictional stress
τ^*	vertical velocity at the top of the boundary layer (N/m^2/sec)
ΔP_δ	Thickness of the boundary layer (mb)
η	nondimensional function of pressure
P	pressure
P_a	pressure of the model atmosphere (N/m^2)
P_s	pressure at the surface (N/m^2)
t	time (sec)
U	eastward wind speed (m/sec)
V	northward wind speed (m/sec)
$\bar{w}$	surface water availability
T	absolute temperature (K)
$\bar{q}_\delta^{(4)}$	heat addition due to water phase changes
g	acceleration due to gravity (m^2/sec)

a	radius of the earth (m)
R	gas constant for dry air (J/Kg/K)
C_p	specific heat of air at constant pressure (J/Kg/K)
k	R/C_p
L	latent heat of condensation (J/Kg)
f	coriolis parameter (rad/sec)
H_s	$= H_{0s}^{(1)} + H_{0s}^{(2)} + H_{0s}^{(3)} + H_{0s}^{(4)} + H_{0s}^{(5)}$ (J/m^2/Sec) = sum of the rates of vertical heat fluxes per unit surface area, directed toward the surface
H_a	$= H_{0a}^{(1)} + H_{0a}^{(2)} + H_{0a}^{(3)} + H_{0a}^{(4)}$ (J/m^2/Sec) = sum of the rates of heat additions to the atmospheric column per unit horizontal area by all processes
$H_{0s}^{(1)}, H_{0a}^{(1)}$	heat flux due to short wave radiation
$H_{0s}^{(2)}, H_{0a}^{(2)}$	heat flux due to long wave radiation
$H_{0s}^{(3)}, H_{0a}^{(3)}$	heat flux due to small scale convection
$H_{0s}^{(4)}$	heat flux due to evaporation
$H_{0a}^{(4)}$	heat flux due to condensation
$H_{0s}^{(5)}$	heat flux due to subsurface conduction and convection
e^*	saturation vapor pressure
R_∞	solar constant (W/m^2)
r_a	albedo of the atmosphere
r_s	albedo of the surface
b_2	empirical constant (J/m^2/sec)
c_2	empirical constant (J/m^2/sec)
e_2	nondimensional empirical constant
f_2	empirical constant (J/m$_2$/sec)
$\bar{k}$	factor proportional to the conductive capacity of the surface medium
a_s	constant used in Sellers model
b_s	positive constant of proportionality used in the Sellers model (kg m^2/J/sec^2)
K_{HT}	coefficient for eddy diffusivity of heat (m^2/sec)
K_{HE}	exchange coefficient for water vapor (m^2/sec)
h	depth of the water column (m)
z	height (m)
V_{0ws}	meridional component of surface current (m/sec)
n	cloud amount
$G_{0,n}$	long wave radiation form the atmosphere for cloud amount "n" (W/m^2)
B_0	long wave radiation from the surface (W/m^2)
$S_{0,n}$	short wave radiation from the atmosphere for cloud amount "n" (W/m^2)
A_n	albedo factor for a cloud amount "n"
R_{f1}	large scale rainfall (mm/day)
R_{f2}	small scale rainfall (mm/day)

1. Introduction

One of the important featues of the tropical circulation is the Inter-Tropical Convergence Zone (ITCZ). The salient features of the observed ITCZ are that (1) the seasonal shift in the latitudinal position of the ITCZ is less over the oceans than over the continents, about $10°-15°$ over the oceans and $20°-25°$ over the continents, (2) the ITCZ over the land follows the seasonal march of the sun and (3) the position of the oceanic ITCZ generally is over the warm regions (Saha, 1971; Estoque and Douglas, 1978; Riehl, 1979). Numerical studies have also shown that the location of the ITCZ depends on the location of the maximum sea surface temperature (Goswami et al., 1984; Pike, 1972).

Another important feature of the tropical circulation is the quasi-periodic oscillations and their northward progression. Yasunari's (1979) spectral analysis of digital cloud intensity in the visible range showed that the cloudiness fluctuation have two dominant periodicities, one around 15 days and another around 40 days. The 15-day and 40-day modes showed northward propagation in the Asian monsoon region. Krishnamurti and Subrahamanyam (1982) analyzed the wind field at 850 mb during MONEX 79. Their extracted $30-50$-day wind component showed steady northward propagation of a trian of troughs and ridges. Observational studies indicate that the tropical monsoon season is characterized by quasi-periodic modes (Sikka and Gadgil, 1980; Krishnamurti, 1986). The $30-50$-day oscillation is considered to be a result of the slow propagation of the Kelvin wave mode which in turn caused by the balance between heating and dissipation (Chang, 1986). This slow Kelvin mode shows a northwest-southeast phase tilt in the northern hemisphere and supports the observed poleward propagation. Later Chang (1986) proposed a Kelvin Wave-CISK mechanism to explain the development and poleward propagation of these low frequency modes. The $10-15$-day oscillation is considered to be a result of the deviations in the stationary oscillations of the basic state (Webster and Chou, 1980). Webster (1983) showed that the quasi-fortnightly oscillations and northward propagation of these fluctuations are the result of land-sea hydrological cycle. Goswami and Shukla (1984) using a symmetric version of GLAS GCM simulated the northward propagation of these fluctuations in the lower atmosphere. Thus the northward progression of these fluctuations has been successfully simulated by several zonally symmetric models. Recently Lau and Lau (1986) using the GFDL GCM showed that there exists east-west propagation of intraseasonal modes in the tropical region and their modulation by seasonal cycle may lead to the northward propagation

of east-west oriented troughs over Asian monsoon region. Most of these studies simulated the observed quasi-periodic modes using numerical models of varying complexity.

In this study an attempt has been made to simulate some of the observed features of the ITCZ and the northward progression of fluctuations during the monsoon period using a simple zonally symmetric global energy balance model. In this model the linear dynamics is treated implicitly. The present model includes various physical and feedback processes using simple relationships.

Energy balance models are some of the simplest mathematical models with many advantages. In spite of the drawbacks due to simplified physics these models provide a tool to study the cause and effect of meteorological phenomena. The heat budget or energy balance models predict the distribution of temperature as a consequence of the balance among various heat fluxes. The associated dynamics is generally parameterized in terms of temperature field. Angular momentum transports are not included. Dynamic parameters are obtained in an empirical manner. One of the advantages of the thermodynamic energy balance models is that they are relatively simple and hence economical on computation time.

In order to achieve the objectives of this study, a zonally averaged energy balance model with prescribed vertical structure is construced. Numerical experiments are then conducted to (i) study the dependency of the migration of the maximum rainfall zone characterized by ITCZ on the meridional surface temperature profile and (ii) study a simple monsoon system that develops as a result of the differential heating between the ocean and continent regimes. Three numerical experiments are performed with an idealized earth-atmosphere system. These are

(i) Global continent domain or Land-covered Planet (LP) experiment,

(ii) Global ocean domain or Ocean-covered Planet (OP) experiment and

(iii) Continent-Ocean domain or Land-Ocean-covered Planet (LOP) experiment with coast running along the equator.

Freezing latitudes (75° to 90°) near the poles are considered in all the three cases. Observations indicate that there exist semiannual cycles of various climatic parameters in the equatorial regions (Reginald et al., 1974). Also the extent of the migration of ITCZ appears to depend on the type of lower boundary conditions (Pike, 1971, 1972). The objectives of the first experiment (LP) are to study the dependence of the migration of the maximum rainfall zone (ITCZ) on the meridional surface temperature distribution and to investigate the existence of any semiannual cycles of different climatic parameters in the equatorial region.

Studies by Pike (1971, 1972) using an interactive ocean-atmosphere primitive equation model suggests that the ITCZ structure over ocean is closely related to the meridional surface temperature distribution over the ocean. Also with an initially constant surface temperature distribution near the equator, Pike (1972) found that a cold equatorial surface developed progressively as a result of upwelling and vertical mixing in the ocean. It appears that in his model these conditions are necessary for the existence and the migration of the oceanic ITCZ.

The objective of the second experiment is to study the migration fo the oceanic ITCZ in relation to the heat transport by the ocean currents. Here two sub-cases are considered; (a) Ocean with no currents (Swamp ocean) and (b) Ocean with wind driven surface currents. Kurihara (1971) has shown that the storage and the meridional transport and hemispheric exchange of energy in the ocean play important roles in determining the state of the climate system.

The observed character of the summer component of the monsoon system may be summarized as the development and organization of cross-equatorial flow. Two specific features of the monsoon region are (1) change in the directin of the prevailing winds by at least 120° between winter and summer and (2) spells of heavy rainfall during the monsoon period. Though there are other features observed the onset and the intensity of monsoon may be characterized by the above the two (Rao, 1976). In the present model these two features are used to define the model's monsoon. Various numerical experiments have revealed that orography (Hahn and Manabe, 1975) and the associated moist processes have important role in the monsoon system (Godbole, 1973). Murakami et al. (1968) found that the neglect of hydrologic processes had little effect on the monsoon system in their model. Webster and Chou (1979, 1983) showed that the mean sesaonal monsoon is determined by differential heating between an in-

teractive ocean and the continent regimes. Their results indicate that the hydrological processes are important to produce the subseasonal variability of the monsoon. Observations also indicate that the monsoon season is characterized by low frequency variability. A time scale of 10 to 15 days and 30 to 50 days with regions of cloud bands are observed to propagate northward across the Southeast Asia (Sikka and Gadgil, 1980). The third experiment (LOP) is designated to simulate the quasi periodic oscillations in a monsoon system.

2. Model Description

2.1 Model Atmosphere Equations

In spherical geometry for an axially symmetric field the vertically averaged thermodynamic energy equation and the water vapor equation for the atmosphere can be written as

$$\frac{\partial \bar{\theta}_0}{\partial t} = -\frac{1}{a\,\mathrm{Cos}\,\varphi}\frac{\partial}{\partial \varphi}\overline{V_0\theta_0}\,\mathrm{Cos}\,\varphi + \frac{1}{a\,\mathrm{Cos}\,\varphi}\frac{\partial}{\partial \varphi}\left(\frac{K_{HT}}{a}\frac{\partial \bar{\theta}_0}{\partial \varphi}\right) + \frac{1}{C_p}\left(\frac{P_s}{P_a}\right)^k \bar{q}_0^{(n)} \tag{1}$$

and

$$\frac{\partial \bar{\varepsilon}_0}{\partial t} = -\frac{1}{a\,\mathrm{Cos}\,\varphi}\frac{\partial}{\partial \varphi}\overline{V_0\varepsilon_0}\,\mathrm{Cos}\,\varphi + \frac{1}{a\,\mathrm{Cos}\,\varphi}\frac{\partial}{\partial \varphi}\left(\frac{K_{HE}}{a}\frac{\partial \bar{\varepsilon}_0}{\partial \varphi}\right) + \frac{g}{P_s}\frac{1}{L}H_{0s}^{(4)} - \frac{1}{L}\bar{q}_0^{(4)} \tag{2}$$

where the double bar represents the vertical average, the subscript "o" represents the zonal average, φ the latitude, θ the potential temperature, ε the humidity mixing ratio, K_{HT} and K_{HE} are coefficients for eddy diffusivity of heat and water vapor. The first two terms on the right side of the above equations are the rate of change due to advection and diffusion and the last term in Eq. 1 is the rate of change due to diabatic processes, and third and last terms in Eq. 2 are source and sink for moisture respectively. A list of symbols is given in the Appendix. Representing the model atmosphere at 500 mb the vertically averaged variables can be written in terms of their values at 500 mb level and at the surface (assumed to be 1000 mb) by prescribing linear profiles except for the vertical velocity for which a parabolic profile is used. Following the relations given by Saltzman and Vernekar (1971), meridional component of Wind V_0, vertical velocity ω_0, atmospheric potential temperature θ_{0a} and humidity mixing ratio ε_0 at pressure level P can be written as

$$V_0(P) = V_{0s}\left(\frac{2P - P_s}{P_s}\right) \tag{3}$$

$$\omega_0(P) = \frac{-\partial V_{0s}\,\mathrm{Cos}\,\varphi}{a\,\mathrm{Cos}\,\varphi\,\partial\varphi}\left[\frac{P(P - P_s)}{P_s}\right] \tag{4}$$

$$\theta_0(P) = \theta_{0a} + (P - P_a)\frac{(\theta_{0s} - \theta_{0a})}{(P_s - P_a)} \tag{5}$$

$$\varepsilon_0(P) = \varepsilon_{0s}\left(\frac{P}{P_s}\right)^{\xi} \tag{6}$$

where $\xi = 2.53$ (in Eq. 6) is an empirical constant suggested by Smith (1966) assumed to be independent of pressure and latitude. The net rate of heat addition to the atmospheric column per unit horizontal area by each diabatic process can be written as (Saltzmann and Vernekar, 1971)

$$H_{0a}^{(n)} = \left(\frac{P_s}{g}\right)\bar{q}_0^{(n)}.$$

Substituting the corresponding relations form Eq. 3, 5 and 6 for the vertically averaged terms in Eq. 1 and 2 and integrating with respect to the pressure, Eq. 1 can be written as the governing equation of the representative atmosphere (500 mb level) as

$$\frac{\partial \theta_{0a}}{\partial t} = \frac{1}{3\,a\,\mathrm{Cos}\,\varphi}\frac{\partial}{\partial \varphi}(V_{0s}\theta_{0a} - V_{0s}\theta_{0s})\,\mathrm{Cos}\,\varphi + \frac{1}{a\,\mathrm{Cos}\,\varphi}\frac{\partial}{\partial \varphi}\left(\frac{K_{HT}\partial\theta_{0a}}{a\,\partial\varphi}\right) + \frac{1}{C_p}\left(\frac{P_s}{P_a}\right)^k \cdot\left[\frac{g}{P_s}(H_{0a}^{(1)} + H_{0a}^{(2)} + H_{0a}^{(3)}) + \bar{q}_0^{(4)}\right] \tag{7}$$

and the governing equation for water vapor at the surface as

$$\frac{\partial \varepsilon_{0s}}{\partial t} = \left[-\frac{\xi}{(1+\xi)(2+\xi)}\frac{1}{a\,\mathrm{Cos}\,\varphi}\frac{\partial}{\partial \varphi}V_{0s}\varepsilon_{0s}\,\mathrm{Cos}\,\varphi + \frac{1}{(1+\xi)}\frac{1}{a\,\mathrm{Cos}\,\varphi}\frac{\partial}{\partial \varphi}\left(\frac{K_{HE}}{a}\frac{\partial \varepsilon_{0s}}{\partial \varphi}\right) + \frac{1}{P_s}\frac{g}{L}H_{0s}^{(4)} - \frac{1}{L}\bar{q}_0^{(4)}\right](1+\xi) \tag{8}$$

where $H_{0a}^{(1)}, H_{0a}^{(2)}, H_{0a}^{(3)}$ are diabatic fluxes. We now deal with the relationships for these fluxes.

Diabatic heating of the atmosphere: The total heating of the atmosphere is given by

$$H_a = \sum_{n=1}^{4} H_{0a}^{(n)} \tag{9}$$

where $n = 1$ represent various contributions to the diabatic heating of the atmosphere as described below. Following the parameterization given by Saltzman and Vernekar (1971), here after referred to as SV, these fluxes can be written as below.

Total short wave flux to the atmosphere, $H_{0a}^{(1)}$ is given by

$$H_{0a}^{(1)} = (1 - r_a)\chi R_0 \tag{10}$$

where χ is the opacity of the atmosphere to the solar radiation, r_a the albedo of the atmosphere and R_0 the intensity of the solar radiation at the top of the atmosphere. Total long wave flux to the atmosphere, $H_{0a}^{(2)}$ is given by

$$H_{0a}^{(2)} = \sigma\left[\Gamma\theta_{0s}^4 - (\gamma_1 + \gamma_2)\left(\frac{P_a}{P_s}\right)^{4k}\theta_{0a}^4\right. \tag{11}$$

where Γ is the emissivity of the lower surface, γ_1 and γ_2 are the climatological factors respectively for downward and upward effective black body long wave radiation from the atmosphere and σ is the Stefan Boltzmann constant. We have taken $\gamma_1 = 1.20$, $\gamma_2 = 0.8$ and $\Gamma = 0.95$ as suggested by SV. First term on the right side of the Eq. 11 represents long wave radiation from the surface and the second term long wave radiation from the atmosphere. Net heat flux due to small scale convection from the lower surface, $H_{0a}^{(3)}$ is given by

$$H_{0a}^{(3)}\left[b_2\left\{\theta_{0s} - \left(\frac{P_a}{P_s}\right)^k\theta_{0a}\right\} + c_2\right] \tag{12}$$

where b_2 and c_2 are empirical constants and are equal to 1.5 Joules/m^2/Sec/°K and -28.0 Joules/m^2/Sec respectively based on observations. Heat flux due to condensation, $H_{0a}^{(4)}$ is given by

$$H_{0a}^{(4)} = \frac{P_s}{g}\bar{q}_0^{(4)} \tag{13}$$

where $\bar{q}_0^{(4)}$ is the rate of heat addition due to condensation. This heat addition in the model is considered to be of two types: (i) large scale precipitation, R_{f1} and (ii) small scale precipitation, R_{f2} assumed to exist only in tropics. The formulations used are as follows.

(i) *Large scale precipitation:* In order to account for the condensation at different levels the atmosphere in the vertical is divided into three layers. Humidity mixing ratio and its saturation values at three levels, i.e., 250, 500, and 750 mb are calculated and corresponding difference between them (only positive values) is treated as the water available for precipitation. The vertical variation of saturated humidity mixing ratio, $\varepsilon_0^*(P)$ is given by

$$\varepsilon_0^*(P) = \frac{0.622}{P}e^*(P)R_h \tag{14}$$

where $e^*(P)$ is the saturated vapor pressure at level P with the following relation:

$$e_0^*(P) = 6.1078\,\mathrm{Exp}\left[\{(T\text{-}273)/(T - b_3)\}a_3\right] \tag{15}$$

where R_h is relative humidity and a_3 and b_3 are empirical constant and are equal to 21.87 and 7.66 over ice and 17.269 and 35.86 over water respectively and are suggested by SV. The mass of water available for large scale precipitation can then be written as

$$R_{f1} = \frac{1}{2g}\int_0^{P_s}\delta\varepsilon(P)\,dP \tag{16}$$

When $\delta\varepsilon(P)$ is positive, R_{f1} is computed and it is assumed that 50% of the excess moisture is precipitated out and the rest is retained to moisten the atmosphere.

(ii) *Small scale precipitation*: In the tropical latitudes convective precipitation is predominant. This convective precipitation is called small scale or cumulus precipitation. A simple empirical formula suggested by Pushitov and Gutman (1970) is used to calculate the small scale rainfall. The latent heat energy input to the atmosphere by convective condensation Φ (assumed to exist between 30 °N and 30 °S) can be written as

$$\Phi = -\eta S\tau^*\bar{W} \tag{17}$$

where η is a function of pressure, S is the stability parameter, τ^* is the vertical velocity at the top of the boundary layer, and $\bar{W}$ the surface water availability. From the continuity equation the vertical velocity at the top of the boundary layer (900 mb)

can be written as

$$\tau^* = \frac{1}{a\,\mathrm{Cos}\,\varphi}\frac{\partial}{\partial\varphi}(V_{0s}\,\mathrm{Cos}\,\varphi)\,\Delta P_\delta \tag{18}$$

where ΔP_δ is the thickness of the boundary layer assumed to be 100 mb. Then the total heating rate Φ due to convective condensation can be written as

$$\Phi = -\frac{\omega(P)}{\omega(P_a)} S\tau^* \bar{W} \qquad \text{for } \tau^* < 0 \tag{19}$$

$$\Phi = 0 \qquad \text{for } \tau^* > 0 \tag{20}$$

and the small scale precipitation, R_{f2} as

$$R_{f2} = \frac{C_p}{g}\frac{1}{L}\int_0^{P_s} \Phi\,\mathrm{d}P. \tag{21}$$

In this model small scale precipitation is considered only in the tropics and neglected in other regions. Heating of the atmosphere due to large and small scale condensations can then be written as

$$\bar{q}_0^{(4)} = (R_{f1} + R_{f2})\frac{gL}{P_s} \tag{22}$$

where L is the latent heat of condensation and P_s the surface pressure.

Parameterization for heat diffusion: An empirical formula suggested by Sellers (1973) is used to calculate the large scale eddy diffusion coefficient for heat, K_{HT} and is given by

$$K_{HT} = C_t|\Delta T|10^6 \tag{23}$$

where ΔT represents the poleward surface temperature gradient and C_t has a value of 0.25. This parameterization is based on the observations presented by Fritz (1960) and Clapp (1970). Analogous to the heat diffusion coefficient K_{HT}, the coefficient for large scale eddy diffusivity of moisture, K_{HE} can be written as

$$K_{HE} = C_e|\Delta\varepsilon|10^6 \tag{24}$$

where $\Delta\varepsilon$ represents the poleward gradient of surface specific humidity and C_e is a weight factor equal to the ratio of the surface humidity mixing ratio at a latitude to the maximum surface humidity mixing ratio. Values of C_e range from zero to unity thus providing a smooth latitudinal distribution of K_{HE}.

2.2 Governing Equations for the Surface

In the present model three types of lower boundary surfaces (land, ocean and ice) are considered. Governing equations for each of them are given below.

The Ocean: Depth-averaged governing equation for the lower surface (ice, water or land) can be written as

$$\frac{\partial\bar{\theta}_{0w}}{\partial t} = \frac{1}{C_s M}H_{0s}^{(n)} - \frac{1}{a\,\mathrm{Cos}\,\varphi}\frac{\partial}{\partial\varphi}\overline{V_{0w}\theta_{0w}} + \frac{1}{a\,\mathrm{Cos}\,\varphi}\frac{\partial}{\partial\varphi}\left(\frac{K_{HW}}{a}\frac{\partial\bar{\theta}_{0w}}{\partial\varphi}\right) \tag{25}$$

where θ_{0w} is the surface potential temperature averaged both zonally and through the depth of the active layer and K_{HW} the coefficient of eddy diffusivity for heat transfer by ocean currents. Following the parameterization given by Sellers (1973) and considering an ocean mixed layer of constant depth h, the depth variation of potential temperature, θ_{0w} can be written as

$$\theta_{0w}(z) = \theta_D + (\theta_{0s} - \theta_D)\,\mathrm{Exp}\,(az) \tag{26}$$

where θ_D is the subsurface temperature at the level of thermocline, and z the depth below the surface. Negative z represents this depth. Depth variation of the meridional current velocity, V_{0w} is then

$$V_{0w}(z) = (1 + \mathrm{az})\,V_{0ws}\,\mathrm{Exp}\,(\mathrm{az}). \tag{27}$$

The surface meridional current velocity, V_{0ws} is taken to be a fraction of the surface zonal wind velocity and is given by

$$V_{0ws} = \mp C_{0w} U_{0s} \tag{28}$$

where $C_{0w} = 0.01$ (Sellers, 1973). Integrating Eq. 25 with respect to depth the governing equation for the ocean surface becomes

$$\frac{\partial\theta_{0s}}{\partial t} = A^{-1}\left\{-\frac{1}{a\,\mathrm{Cos}\,\varphi}\frac{\partial}{\partial\varphi}\mathrm{Cos}\,\varphi\left[\theta_D V_{0ws}\,\mathrm{Exp}\,(-ah) + (\theta_{0s}-\theta_D)V_{0ws}\left\{\frac{A}{4}+\frac{\mathrm{Exp}(-2ah)}{2}\right\}\right] + \frac{1}{C_s M}H_{0s}^{(n)} + \frac{1}{a\,\mathrm{Cos}\,\varphi}\frac{\partial}{\partial\varphi}K_{HW}\frac{\partial}{a\,\partial\varphi}[\theta_{0s}A + \theta_D(1 - A^{-1})]\right\} \tag{29}$$

where

$$A = \left[\frac{1 - \mathrm{Exp}(-ah)}{ah}\right]$$

Surface heat fluxes: The net heat transfer at the surface is given by

$$H_s = \sum_{n=1}^{5} H_{0s}^{(n)} \tag{30}$$

where $n = 1$ to 5 represents various heat fluxes. Following the parameterizations given by SV, different heat fluxes can be written as below.

Net short wave radiation flux to the surface, $H_{0a}^{(1)}$ is given by

$$H_{0s}^{(1)} = (1 - r_a)(1 - \chi)(1 - r_s) R_0 \tag{31}$$

where r_s the surface albedo, r_a the atmospheric albedo and R_0 the intensity of the solar radiation at the top of the atmosphere. Net long wave radiation flux to the surface, $H_{0s}^{(2)}$ is given by

$$H_{0s}^{(2)} = \sigma\left[\gamma_1\left(\frac{P_a}{P_s}\right)^{4k} \theta_{0a}^4 - \theta_{0s}^4\right] \tag{32}$$

Assuming that the amount lost (gain) by the atmosphere will be the gain (loss) to the surface, the sensible heat flux, $H_{0s}^{(3)}$ is taken to be

$$H_{0s}^{(3)} = -H_{0a}^{(3)}. \tag{33}$$

Heat flux due to the evaporation at the surface, $H_{0s}^{(4)}$ is given by

$$H_{0s}^{(4)} = \bar{W}\,[e_2 H_{0s}^{(3)} + f_2] \tag{34}$$

where e_2 and f_2 are dimensionless empirical constants and $\bar{W}$ is surface water availability. Thus heat flux due to evaporation is made dependent on sensible heat flux. Heat flux due to sub-surface conduction and convection, $H_{0s}^{(5)}$ is given by

$$H_{0s}^{(5)} = -\bar{k}\,(\theta_{0s} - \theta_D) \tag{35}$$

where $\bar{k}$ is a factor for the conductivity of the surface.

2.3 Governing equation for the Land and Ice Surfaces

When the lower surface is a rigid one (ice or land) the advection term for these surfaces drops out from Eq. 29 and neglecting the diffusion the governing equation for the surface can be written as

$$\frac{\partial \theta_{0s}}{\partial t} = \frac{1}{C_s M} H_{0s}^{(n)}\left[\frac{1 - \mathrm{Exp}(-ah)}{ah}\right]^{-1} \tag{36}$$

2.4 Wind and Temperature Relationships near the Surface

Approximate expressions for the surface wind velocity components within the friction layer can be derived from the momentum equations,

$$fV_{0s} + a_{0s}\frac{\partial}{\partial z}\tau_{0xs} = 0 \tag{37}$$

$$fU_{0s} - a_{0s}\frac{\partial}{\partial z}\tau_{0ys} + a_{0s}\frac{\partial}{a\,\partial\varphi}P_{0s} = 0 \tag{38}$$

where τ_{0xs} and τ_{0ys} are the Eastward and Northward components of the frictional stress, and a_{0s} is the specific volume at the surface. Assuming a logarithmic wind profile relationship near the surface and using the equation of state to approximate the pressure gradient term proportional to the surface temperature gradient, these equations can be written as

$$fV_{0s} - a_s |U_{0s}| U_{0s} = 0$$

$$fU_{0s} + a_s |V_{0s}| V_{0s} + R(1 - b_s)\frac{\partial \theta_{0s}}{a\,\partial\varphi} = 0.$$

Solving for the surface wind components gives (Sellers, 1973) at any latitude:

$$U_{0s} = \frac{\left[R(b_s - 1)\dfrac{\partial \theta_{0s}}{a\,\partial\varphi}\right]}{f\left[1 + \left|\dfrac{a_s U_{0s}}{f}\right|^3\right]}$$

$$V_{0s} = \frac{a_s}{f}|U_{0s}|\,U_{0s} \tag{39}$$

and at the equator:

$$U_{0s} = 0 \text{ and } V_{0s} = \sqrt{\left[\frac{R}{a_s}(b_s - 1)\frac{\partial \theta_{0s}}{a\,\partial\varphi}\right]}$$

2.5 Feedback Processes and Surface Parameters

The feedback processes due to the clouds, albedo, and soil moisture in the model are given below.

(a) *Cloud amount* (n): The cloud amount n, can be calculated as the ratio of the rainfall over a latitude, R_f to the maximum rainfall, $R_{f\,max}$. The climatological values of the total cloud amount varies from 0 to 0.5. Calculated cloud amount is reduced by a factor of two to conform to these

values and can be written as

$$n = 0.5\left(\frac{R_f}{R_{f\,max}}\right) \tag{40}$$

(b) *Long wave radiation-Cloud feedback*: Making use of a simple empirical relation suggested by Kondetreyev (1969), the increased atmospheric long wave radiation emission for a cloud amount n can be written as

$$G_{0,n} = G_0(1 + C'n) \tag{41}$$

Here G_0 is the downward directed long wave radiation from the atmosphere with clear skies, and $C' = c(B_0/G_0 - 1)$ where B_0 is long wave radiation from the surface and c is a constant, equal to 0.76.

(c) *Short wave radiation-Cloud feedback*: The decreased short wave radiation for a cloud amount n can be written as (Kondetreyev, 1969)

$$S_{0,n} = H_{0a}^{(1)}(1 - A_n) \tag{42}$$

where $H_{0a}^{(1)}$ is the incoming solar radiation with clear skies and the parameter $A_n = n \cdot a_k$, with $a_k = 0.7$.

(d) *Surface water availability* ($\bar{W}$): Considering a soil depth of one meter as the active depth and assuming that 50% of the volume is occupied by voids, it follows that 500 mm of water is enough to saturate the soil. The water availability over the land surface can then be written as

$$\bar{W} = \frac{S_m}{H_d P^0}, \qquad 0 \lesssim \bar{W} \lesssim 1 \tag{43}$$

where S_m is the soil moisture, H_d is depth of the active layer and P^0 the porosity of the soil. Over ocean, $\bar{W}$ is assumed to be unity and over the ice zero.

(e) *Soil moisture* (S_m): Neglecting the surface run off, the soil moisture over the land surface, S_m can be considered as the balance between the rainfall, evaporation and the existing soil moisture (S_{me}) given by

$$S_m = (R_f - E_v) + S_{me} \tag{44}$$

where R_f is the total rainfall and E_v the evaporation at the surface.

(f) *Surface density* (ρ_{sws}): The density of ocean water and ice are taken as constants. The soil density is made a function of surface water availability. Wet soil density, ρ_{sws} is then

$$\rho_{sws} = \frac{(\rho_{sd} + e\,\rho_w \bar{w})}{1 + e} \tag{45}$$

where e is the void ratio, assumed as 0.5, and ρ_{sd} and ρ_w are the densities of dry soil and water, respectively. Here a dark type of soil is considered with a density, $\rho_{sd} = 1\,600\,\mathrm{kg/m^3}$.

(g) *Surface specific heat* (C_{sws}): Since the soil specific heat is a function of the wetness and density, the surface specific heat is given by

$$C_{sws} = \frac{C_{sd} + e\,C_w \bar{W}\dfrac{\rho_w}{\rho_{sd}}}{1 + \dfrac{\rho_w}{\rho_{sd}}\bar{w}\,e} \tag{46}$$

where C_{sd} and C_w are the specific heats of dry soil and water respectively, and ρ_w and ρ_{sd} are the densities of water and dry soil respectively. The values used are given in Table 1.

(h) *Surface Albedo* (r_s): Over the ocean and ice regions constant surface albedos are assumed and are 0.06 and 0.8, respectively. Over land it can be calculated as

$$r_s = r_{sd}(1 - \bar{W}) + r_{sws}\bar{W} \tag{47}$$

where r_{sd} and r_{sws} are the albedos of dry soil and wet soil and are equal to 0.28 and 0.15, respectively (Sellers, 1965).

2.6 Ice Cover

Following Budyko (1969), a simple feedback process is used, which assumes that the ice line is

Table 1. *Various Constants Used in the Model Equations*

k	$= R/C_p = 0.287$	a_k	$= 0.76$
P_s	$= 10^5$ N m^{-2}	P^0	$= 0.5$
P_a	$= 5 \times 10^4$ N m^{-2}	e	$= 0.5$
χ	$= 0.3$ (0.55 over ice)	ρ_{sd}	$= 1\,600\,\mathrm{kg\,m^{-3}}$
σ	$= 5.67 \times 10^{-8}$ J m^{-2} S^{-1} K^{-4}	ρ_w	$= 1\,000\,\mathrm{kg\,m^{-3}}$
Γ	$= 0.95$	C_{sd}	$= 2\,000\,\mathrm{J\,kg^{-1}\,K^{-1}}$
γ_1	$= 1.2$	C_w	$= 4\,200\,\mathrm{J\,kg^{-1}\,K^{-1}}$
γ_2	$= 0.8$	r_{sd}	$= 0.28$
b_2	$= 1.5$ J m^{-2} S^{-1} K^{-1}	r_{sws}	$= 0.15$
c_2	$= 28.0$ J m^{-2} S^{-1}	ΔP_δ	$= 100$ mb
ξ	$= 2.58$	z	$= 100$ m (for water)
a	$= \pi/h$	C_{0w}	$= 0.01$
e_2	$= 1.27$	f_2	$= -32.0$

determined by a threshold surface temperature. Initially we assume an ice of thickness two meters over the latitudinal belts between 75° and 90°. If the surface temperature falls below the threshold temperature (273 °K), then the model assumes that the lower surface is covered by ice.

2.7 Solar Radiation

Intensitivity of the Solar radiation at the top of the atmosphere over any latitude can be written as

$$R_0(\varphi, t) = \frac{R\infty}{\pi}[H \operatorname{Sin}\varphi \operatorname{Sin}\delta + \operatorname{Cos}\varphi \operatorname{Cos}\delta \operatorname{Sin} H] \quad (48)$$

where δ the solar declination, $R\infty$ the solar constant, H the hour angle in radians between sunrise or sunset and solar noon, φ the latitude. Here

$$\delta = 23.5° \operatorname{Sin} 2\pi\left[\frac{n_t \cdot \Delta_t}{A_s}\right] \quad (49)$$

and

$$H = \operatorname{Cos}^{-1}(-\tan\varphi \tan\delta) \quad (50)$$

with n_t as the number of time steps, A_s the number of seconds in a year, and Δt the time step in seconds.

3. Numerical Experiments

Using the annual zonally averaged values of climatic data (Reginald et al. 1974) for the input parameters, u_{0s}, v_{0s}, θ_{0s}, θ_{0a} and r_s, three numerical experiments are performed. The time integration is carried out for twenty years for all the three cases. These numerical experiments are (i) Continent domain experiment (referred to as LP or Land-covered Planet experiment) (ii) Ocean domain experiment (referred to as OP or ocean-covered Planet experiment) and (iii) Continent-Ocean domain experiment (referred to as LOP or Land-Ocean-covered Planet experiment) with freezing latitudes (75° to 90°) near the poles. With grid resolution of 5° and 360 days in a year (remaining 5.25 days were adjusted in the time step), a time step of 6.0875 hours is used. This time step satisfies the diffusion and C.F.L. criteria. Monthly (30 days) averages and the daily values of the 20th year of integration are analyzed and the results are presented in the following section. Day 1 in all the time series plots corresponds to the spring equinox of the twentieth year of integration unless other wise indicated. The plots of latitudinal distribution of various parameters are for July and January mean conditions. The model simulations, with atmosphere at rest, for the first the two experiments (LP and OP experiments) are comparable with that of Kuihara (1971). At 85° and 90° latitudes the potential temperature gradients were made equal to zero so that no flux across the poles exists.

4. Discussion of Results

4.1 Land-Covered Planet (LP) or Continent Domain Experiment

Figures 1 (a), (b), and (c) show the monthly averages of surface potential temperature at 0°, 45°

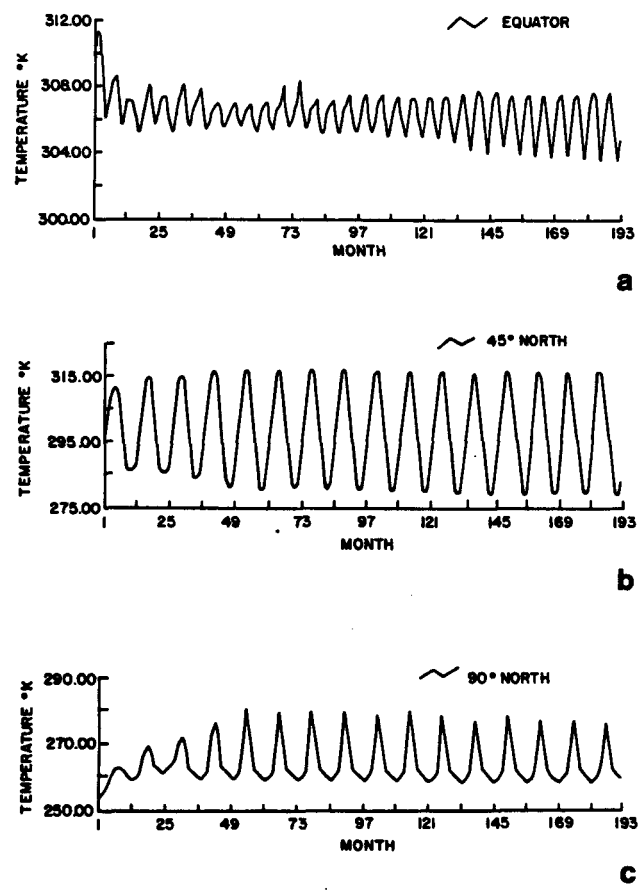

Fig. 1 a, b, c. Time variation of surface temperature at 0°, 45° and 90° North for the Land-Planet (LP) experiment, beginning with spring equinox of the first year of time integration. Semi-annual cycles are found over the equator

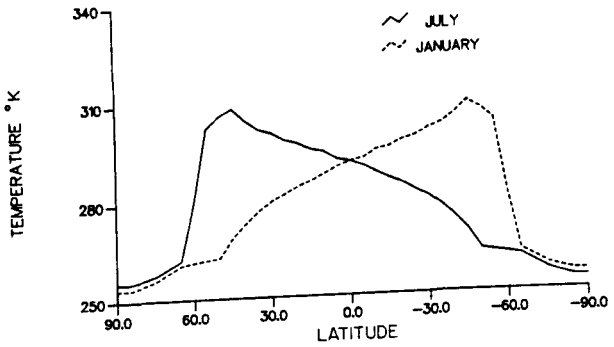

Fig. 2. Latitudinal variation of surface potential temperature for twentieth year (LP)

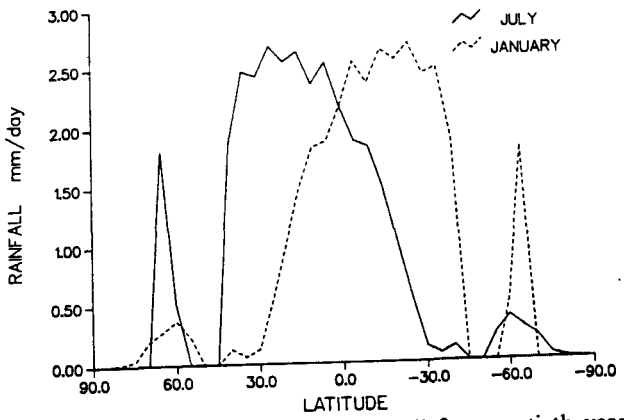

Fig. 3. Latitudinal variation of rainfall for twentieth year (LP). The maximum rainfall zone (ITCZ) migrates 25° poleward with seasons

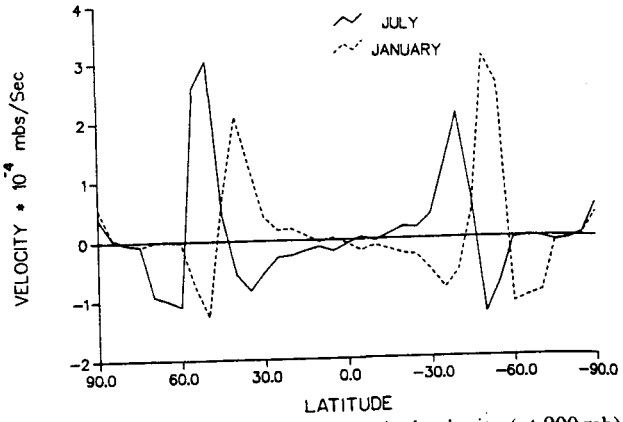

Fig. 4a. Latitudinal variation of vertical velocity (at 900 mb) for twentieth year (LP)

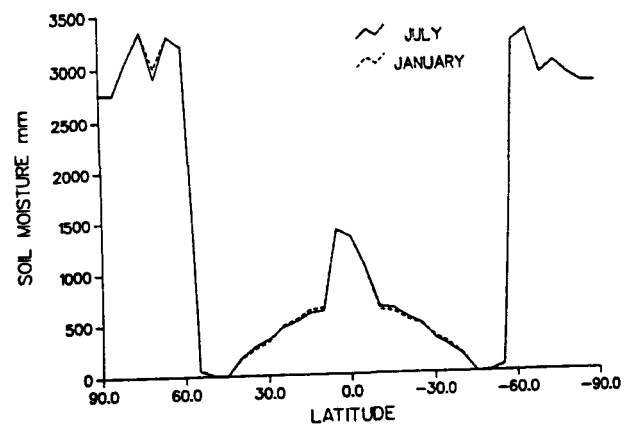

Fig. 4b. Same as in Fig. 4a but for soil moisture. Desert regions are found over zero soil moisture zones

and 90 °N respectively plotted for sixteen years. The number on the abscissa are the months beginning with spring equinox. From the Fig. 1 it can be seen that at 45° and 90 °N the climatic values repeat after third year of integration where as at the equator the climatic values repeat only after the twelfth year of integration. This indicates that the climatic processes over the equatorial region could be more complex than those at other latitudes. Over the equatorial regions semiannual cycles are observed with double maxima lagging behind the insolation maxima by one month. There are no such semi-annual cycles over other latitudes. This result is in agreement with the climatic observations showing the existence of intra-annual cycles of temperature and other parameters over the equatorial regions (Reginald et al., 1971). Latitudinal distributions of surface potential temperature for July and January are shown in Fig. 2. The surface potential temperature maximum shifts to 45° north and 45° south with seasons. The atmospheric potential temperature (not shown) also shows the same feature. Figure 3 shows the migration of the ITCZ indicated by maximum rainfall and this migration is up to 25° north and south with seasons. Observations also show similar poleward limit of the ITCZ with seasons over the continents (Estoque and Douglas, 1978; Riehl, 1979). Model results indicate no rainfall over the latitudinal belt between 45° and 55°. The surface humidity mixing ratio is very low (close to zero) over these dry regions. Figures 4 (a) and (b) show the distribution of vertical velocity at 900 mb (which is assumed to be the level of the top of the boundary layer) and soil moisture respectively with latitude. Over the dry belt, 45° to 55° latitude, strong sinking motion prevails and the soil moisture is zero. These dry belts represent the model's desert regions. This result is in qualitative agreement with

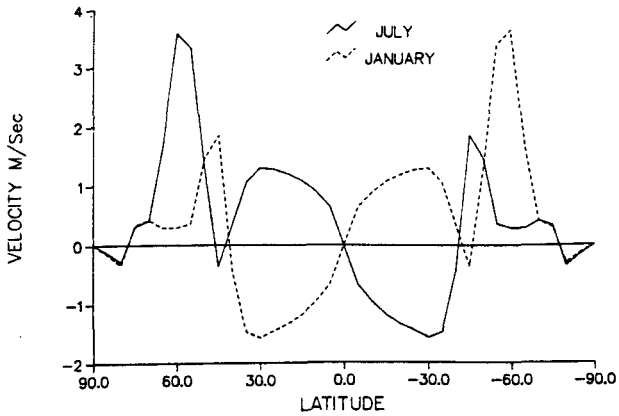

Fig. 5. Latitudinal variation of surface zonal wind velocity for the twentieth year (LP)

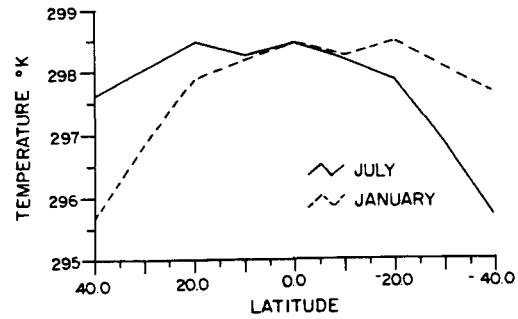

Fig. 6. Latitudinal variation of surface potential temperature for the wind driven Ocean (WO-OP) for twentieth year. Double temperature maxima with a dip in between is found to migrate 5° poleward with seasons

the fact that most of the deserts are found between 30° to 45° over both the hemispheres. Small poleward extension of the deserts in the model could be due to the assumption of simplified distribution of the continental mass. Slight asymmetric distribution of the soil moisture is caused by the asymmetric distribution of the evaporation (not shown) at the surface. Figure 5 shows the variation of the zonal component of the surface wind with latitude. During the northern hemispheric summer solstice the easterlies from the southern hemisphere cross the equator and become westerlies over the tropical region. Reverse pattern is observed over the southern hemisphere during the southern hemispheric summer solstice. Existence of a single Hadley cell during these periods is thus evident.

4.2 Ocean-Covered Planet (OP) or Ocean Domain Experiment

Two numerical experiments with ocean domain are performed. In the first experiment a swamp ocean, i.e., ocean with no currents is considered. In this case the interaction between the atmosphere and the ocean is only through diabatic heat fluxes. Initially a symmetric surface temperature distribution with a single maximum over the equator has been considered as a starting condition. The time integration is carried out with variable solar forcing for twenty years. In the second experiment wind-driven surface currents are generated in the ocean to accomplish the heat transport by the ocean currents and again the time integration is carried out for twenty years. The basic purpose of this experiment is to determine whether the migration of the oceanic ITCZ depends on the meridional surface temperature distribution and to investigate the role of the heat transport by ocean currents on the migration of the ITCZ. We now refer the swamp ocean case as SO-OP and the wind driven ocean case as WO-OP. Figure 6 shows the latitudinal distribution of surface temperature for wind driven ocean case. In the SO-OP case the surface temperature changes with seasons but the temperature maximum over the equator does not shift poleward (not shown). In the WO-OP case a double maxima of surface temperature with a dip in between exists and this migrates 5° north and south with seasons (Fig. 6). Pike (1971, 1972) using an interacting ocean and atmospheric primitive equation model showed that a cold equatorial ocean surface appears and a single ITCZ develops north or south of the equator over the surface temperature maximum in the warmer hemisphere. Pike (1971, 1972) also found that the dip in the temperature over the equatorial region developed as a result of the upwelling and vertical mixing in the ocean and the ITCZ migrated quickly between the hemispheres lagging slightly behind the seasonal reversal of the surface temperature asymmetry. His model's ITCZ migration was clearly related to the seasonal progress of the surface temperature. The magnitude of the dip in the equatorial surface temperature in the present study is low (less than 0.5° K) as compared to the one reported by Pike (5.0° K). The lower value is believed to be due to the lack of the multiple ocean layers and the assumption of simple ocean dynamics in the model. These features may

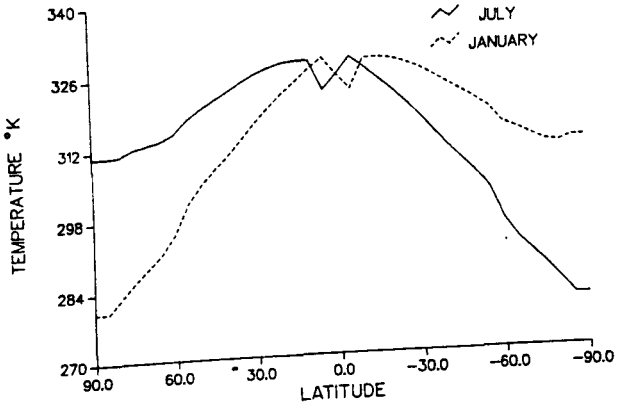

Fig. 7. Same as in Fig. 6 but for atmospheric potential temperature for twentieth year (WO-OP)

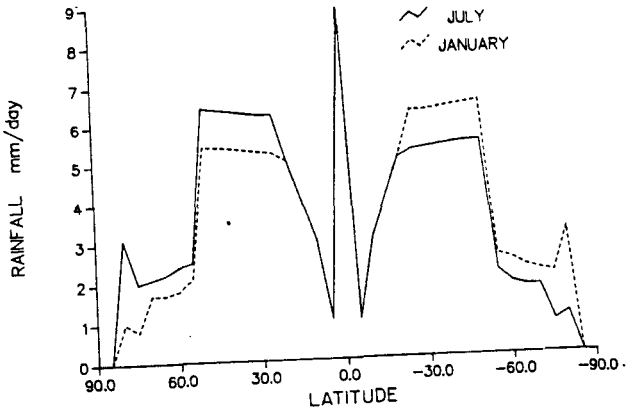

Fig. 8 a. Latitudinal variation of rainfall for twentieth year for the Swamp Ocean (SO-OP). Rainfall maximum (ITCZ) does not show any seasonal migration

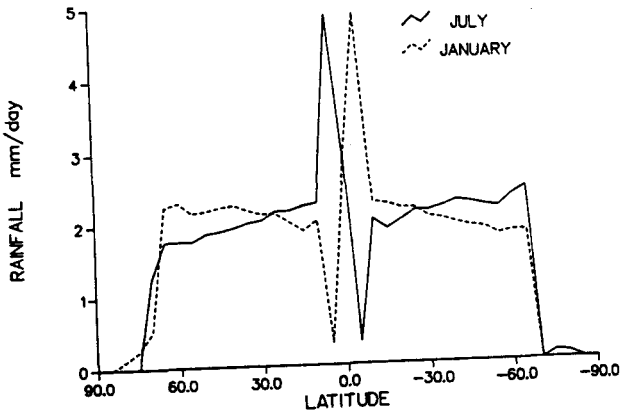

Fig. 8 b. Latitudinal variation of rainfall for twentieth year for the wind-driven ocean (WO-OP). ITCZ migrates 5° poleward with seasons

be important in determining the thermal state of the oceans. Moreover, in the present model the subsurface temperature at the level of the thermocline which determines the direction of the vertical heat transfer at the subsurface due to conduction and convection is held constant with time. This decrease in the surface potential temperature field is believed to be due to large evaporation at the surface. Figure 7 shows the model atmospheric potential temperature variation with latitude for the wind driven ocean (WO-OP) case. A decrease of about 6° K is found even in the atmospheric potential temperature for the WO-OP case. The location of the dip in the mean atmospheric potential temperature coincides with the location of maximum cloudiness (not shown here) and also with the peaks of rainfall and vertical velocity patterns. A similar dip in the humidity field (not shown here) is also found. Figures 8 (a) and (b) show the latitudinal variation of rainfall with seasons for the swamp ocean (SO-OP) and wind driven ocean (WO-OP) cases respectively. In the SO-OP case there exists a single rainfall maximum just over the equator all the time. The rainfall maximum in WO-OP case migrates 5° north and south with seasons. The rainfall minima on both sides of the single maximum in the Fig. 8 (a) are caused by the sinking branches of Hadley cells on both hemispheres with a common rising limb over the equator. The rainfall maximum next to the rainfall minimum in the Fig. 8 (b) is due to the single Hadley cell with a rising limb over warmer hemisphere and with a sinking limb over the cooler hemisphere. In WO-OP case during July and January the Hadley cells merge into a single cell with one rising and one sinking limb. Figure 9 shows the variation of vertical velocity (at the top of the boundary layer, 900 mb) with latitude for the WO-OP case. Strong vertical motions over 5° N during July and 5° S during January are consistent with the rainfall maximum over these latitudes. Figure 10 shows the latitudinal variation of the zonal component of the surface wind. The model results concerning the tropical easterlies, strong westerlies in the middel latitudes and weak polar easterlies are in accordance with the observed general pattern.

From the above results of LP and OP experiments it is apparent that the migration of the ITCZ strongly depends on the meridional surface temperature distribution. The meridional transport o

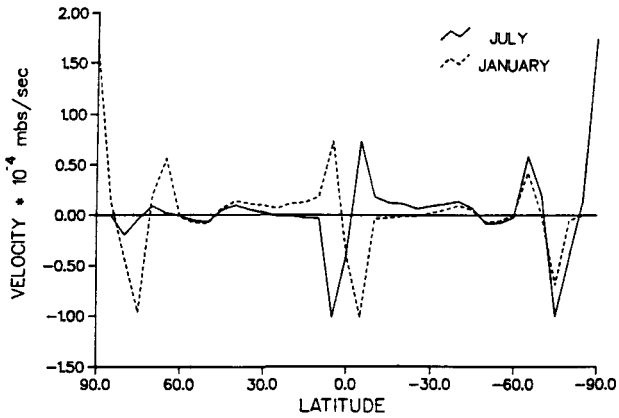

Fig. 9. Latitudinal variation of vertical velocity (at 900 mb) for the twentieth year for the wind-driven Ocean-Planet (WO-OP)

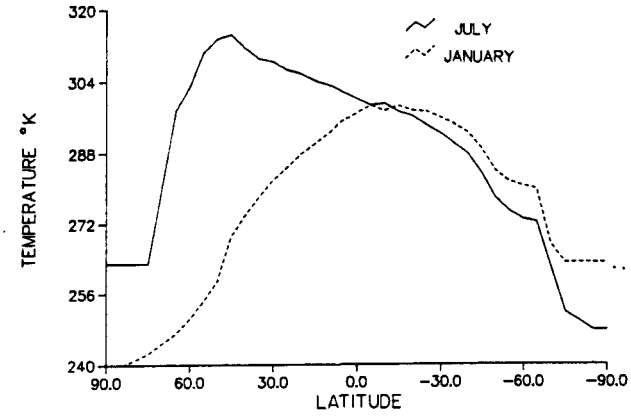

Fig. 11. Latitudinal variation of surface potential temperature for the twentieth year for the Land-Ocean covered Planet (LOP)

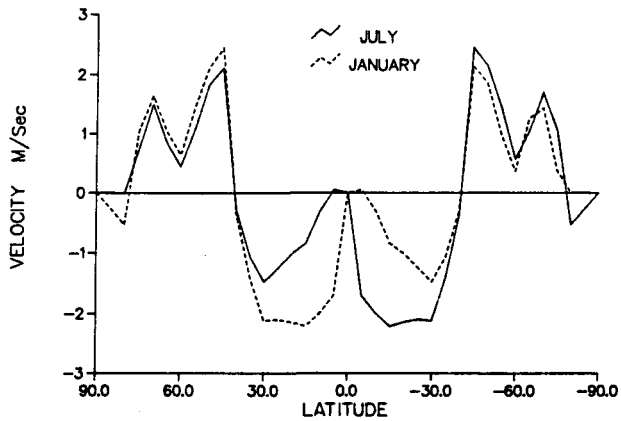

Fig. 10. Latitudinal variation of surface zonal wind velocity for the twentieth year for the wind-driven Ocean-Planet (WO-OP)

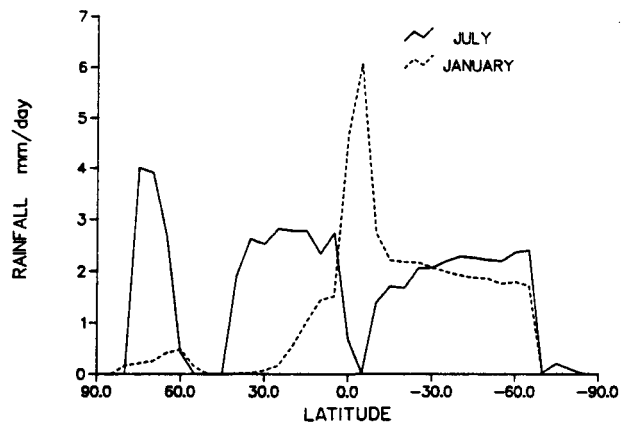

Fig. 12. Latitudinal variation of rainfall for the twentieth year for LOP experiment. Over land ITCZ shifts up to 25° North and over wind driven ocean it shifts up to 5° South

heat by ocean currents appears to be an important process. At least over the ocean, ITCZ migration is associated with the double maximum of surface potential temperature. The extent of the migration of the oceanic ITCZ strongly depends on the location of the maximum ocean surface temperature. In contrast, over the land even though the surface temperature maximum shifts 45° poleward, the ITCZ shifts only 25° poleward.

4.3 Land-Ocean-Covered Planet (LOP) or Continent-Ocean Domain Experiment

An idealized continent-ocean system with the continental cap north of the equator and the ocean south with the coast running along the equator is considered. Initially latitudes near the poles from 75° to 90° are assumed to be covered with ice. The extent of the ice is determined by a threshold surface temperature. Time integration is carried out for the twenty years with seasonally varying solar forcing.

Figure 11 shows the latitudinal variation of the surface potential temperature. Over the continent the maximum is at 45° N during July. Over the ocean, during January, the maximum is at 15° S. Figure 12 shows the latitudinal distribution of rainfall. There is no rainfall at the 45° – 55° latitude belt and during January this dry belt extends up to 35° N towards the equator. Strong sinking motions are found over this dry latitudinal belt. This dry belt with sinking motion represents the mo-

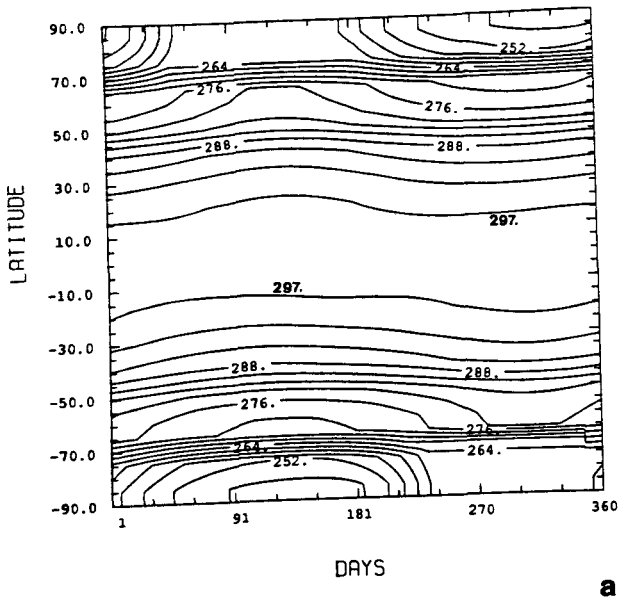

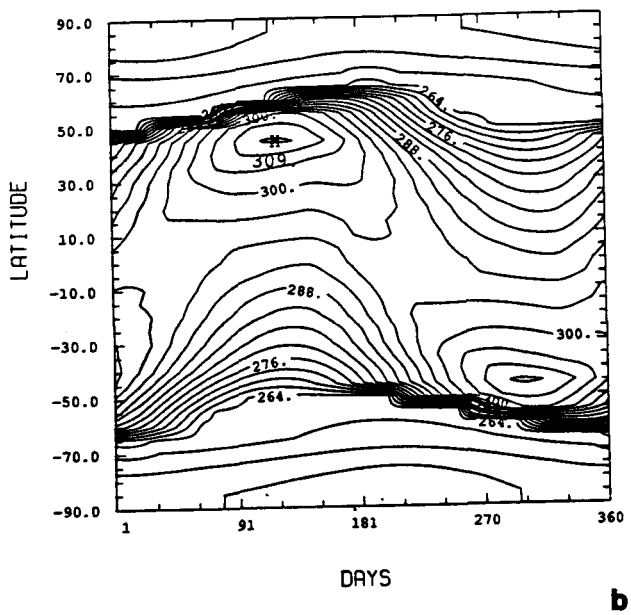

Fig. 13 a, b. Time-Latitude section of surface potential temperature for OP and LP experiments beginning with spring equinox of 20th year of integration. Contour interval: 3° K. Smooth seasonal variation is found

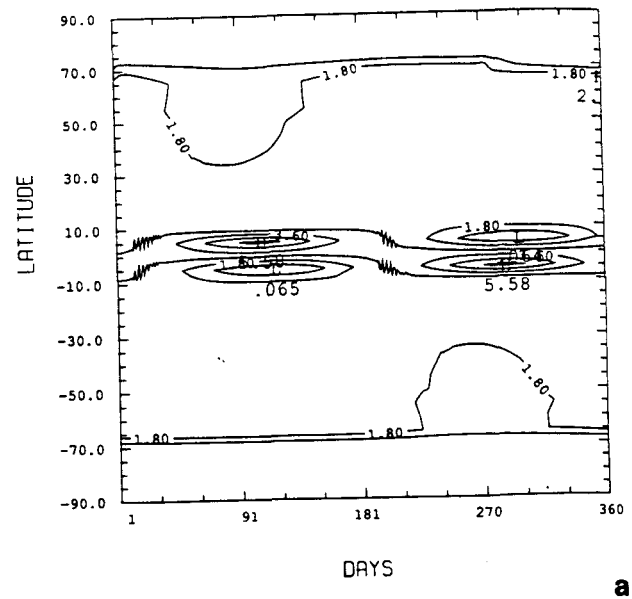

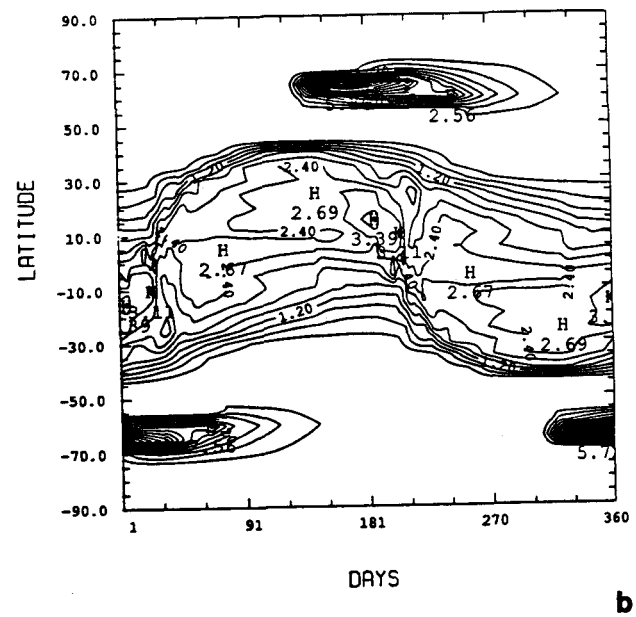

Fig. 14 a, b. Same as in Fig. 13 but for rainfall. Contour interval: 9 mm and 3 mm for OP and LP experiments respectively

del's desert region. Figures 13 (a) and (b) show the smooth seasonal variation of the surface potential temperatures for the ocean-covered (OP) and landcovered (LP) domains respectively. Figures 14 (a) and (b) show the rainfall distribution for the OP and LP domains respectively. No cellular type of structure is seen in both the OP and LP domains. Figure 15 depicts the time-latitude section of vertical velocity (at 900 mb) starting with spring equinox of the twentieth year of time integration. A cellular type structure can be seen over tropical latitudes. An "epoch" as termed by Sikka and Gadgil (1980) or an "event" as termed by Webster (1983) is apparent in Fig. 15 as cells of strong vertical motions moving northward with time. A weak event appears South of the equator

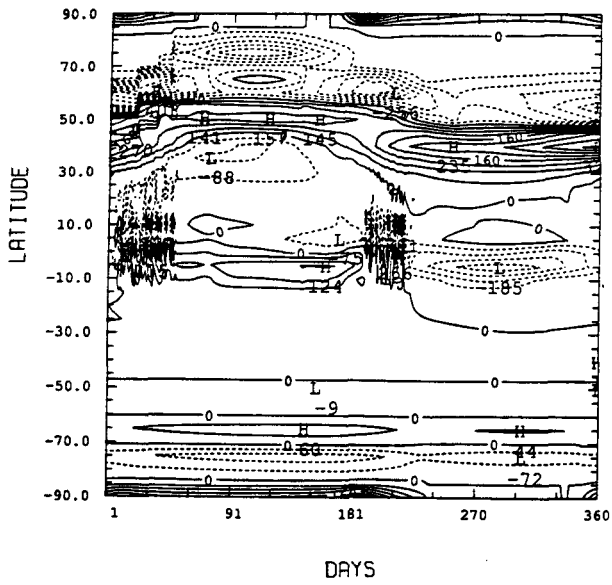

Fig. 15. Time-latitude section of vertical velocity (at 900 mb) for LOP experiment beginning with spring equinox of the 20th year of integration. Scale: 10^{-6} mb. Contour interval: 40×10^{-6} mb. Dashed contours represent negative values. Subseasonal activity and northward propagation of "events" with a period of 8 to 15 days can be seen

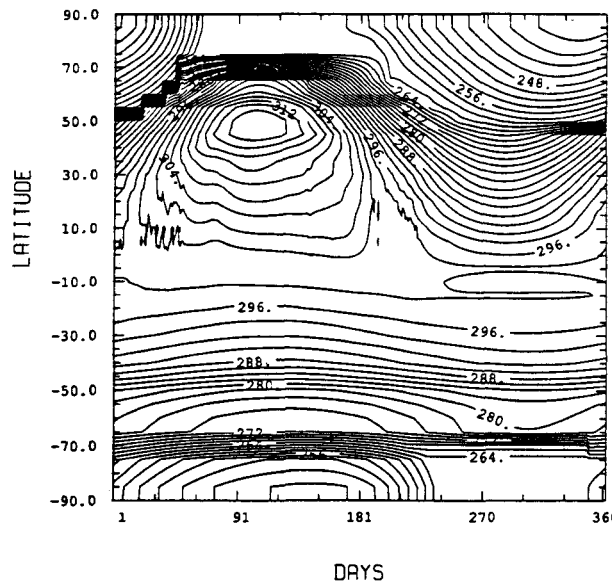

Fig. 16. Same as in Fig. 15 but for surface potential temperature (LOP). Contour interval: 2° K. Oscillations are found during pre-monsoon season

during April. During May and June these "events" propagate northward while a new "event" originates in the lower latitudes. During July and August a well defined strong vertical motion appears over 35° N where the "events" merge and lose their identity. Even though two new "events" originate north of the equator during June to mid July and during mid August to September, these events do not show any northward movement. The poleward excursion of these events disappears once there exists a period of strong and well defined vertical motion over middle latitudes. Again in late September these events appear over 15° N of the coast.

Webster (1983) using a zonally symmetric primitive equation model showed that these "events" are present during the entire monsoon season and disappear during the other seasons. In the present model the poleward excursion of the "events" disappears once there exists a period of strong and well defined rising motion over the middle latitudes. Webster and Chou (1979 a) also found that these "events" were absent in the global ocean experiment and even in the ocean-continent experiment. But the "events" appeared only in the ocean-continent experiment when hydrological processes are considered.

We also find that these events are absent in the land-covered planet (LP) and ocean-covered planet (OP) experiments even in the presence of hydrological processes similar to that of Webster and Chou (1979 b). "Events" exist only in the LOP experiment where hydrological processes and differential heating due to land-ocean contrasts exist. These two processes are obviously necessary for the existence of the "events" in the present model.

Figure 16 shows the distribution of surface potential temperature over different latitudes. Strong rising motions over the land and over the ocean occur over the locations of the surface potential temperature maxima. During April and May quasi-periodic oscillations associated with the "events" are seen in the surface temperature field over the tropical latitudes (Fig. 16) and is in agreement with the results reported by Webster (1983). The period of oscillations for the vertical velocity field and for the surface temperature field are about 8 to 15 days. The observational and the numerical studies by Sikka and Gadgil (1980), Murakami (1977), Krishnamurti and Bhalme (1976) show that there exist two principal energy peaks with 10–15 days and 30–40-day periods. But in the present model results there is no indication of 30–40-day oscillations.

Time-latitude of rainfall for 360 days after spring equinox is shown in Fig. 17. The regions

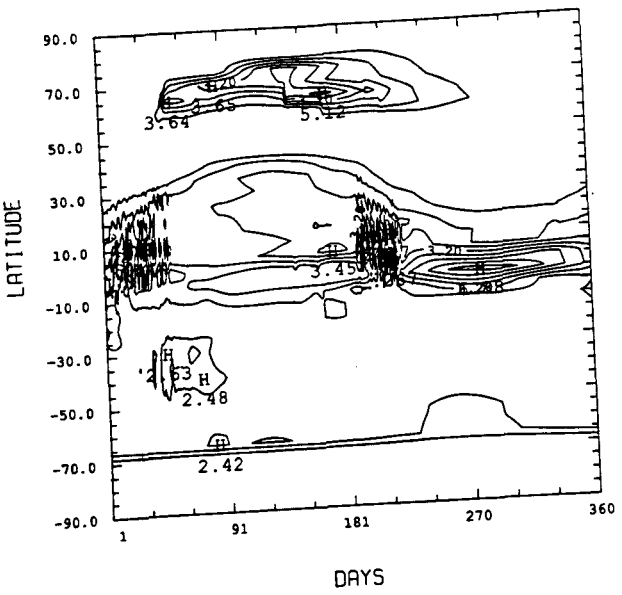

Fig. 17. Same as in Fig. 15 but for rainfall (LOP). Spells of rainfall with periods of 8 to 15 days is found. Contour interval: 0.8 mm

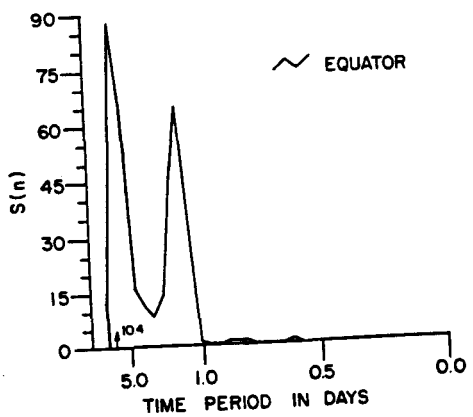

Fig. 18. Spectral plot of rainfall at equator (LOP) during the pre-monsoon season. Dominant rainfall is in the period of 10.4 days

and the periods of rising motion are well correlated with the regions and the periods of rainfall. Figure 18 shows the spectral plot of the rainfall at the equator for two months starting from spring equinox. A peak in the 10–11-day period is clearly seen. The secondary peak corresponds to the rainfall with a period of 1.4 days. Figures 19 (a), (b) and (c), (d) show the time series plots of vertical velocity (at 900 mb), and surface potential temperature for a 60-day period starting with spring equinox at 10° N and 15° N respectively. Figure 19 (e) shows the rainfall at 10° N for the same period and the magnitude of the peaks in the rainfall rate increases by a factor of about 5 as compared to the rainfall before the 60-day period. This type of rainfall pattern is typical during the time of summer monsoon (Rao, 1976). These peaks repeat with a period of about 8 – 13 days in surface temperature, vertical velocity and rainfall fields. The time periods associated with these peaks are in good agreement with the dominant frequency obtained using the spectral analysis of the rainfall shown in the Fig. 18. Figure 20 (a) shows time series plot of surface temperature, vertical velocity, sensible heat flux and latent heat flux at 15° N for the 60-day period starting from the spring equinox. For the sake of analysis the magnitudes of all components on y-axis are not shown. It can be seen that the peaks in the surface potential temperature are in phase with those of the sensible heat flux. Peaks in the vertical velocity are in phase with those of the latent heat flux and both these fields lag behind that of the surface potential temperature. Figure 20 (b) shows the similar trend in these parameters at 20° N. Thus a perturbation in the surface potential temperature field appears to cause a change in the sensible heat flux field which in turn produces perturbations in the vertical velocity and latent heat flux fields.

Temporal and latitudinal distribution of the parameters discussed above can provide more insight into the mechanism of development of these oscillations. Figure 21 (a) to (f) show the latitudinal distribution of vertical velocity, latent heat flux, sensible heat flux and surface potential temperature over the latitudes 0° – 30° N for the days 11 through 26 starting from spring equinox. One day 11 the vertical velocity maximum is located over 10° N and by day 20 this has migrated to 20° N with a secondary maximum at 5° N. Again by day 26 the secondary maximum at 5° N has moved to 10° N with a reduction in the amplitude. On day 11 the zone of maximum condensation (latent heat flux) is at 10° N. By day 23 the magnitude of latent heat flux decreases at 10° N, but increases relatively at 20° N. By day 26 the pattern resembles close to that on day 11. Though the relative amplitudes of the propagating latent heat flux peaks are decreasing during the poleward propagation this is essentially similar to the poleward propagation of the vertical velocity peaks. On day 11 the surface temperature maximum is

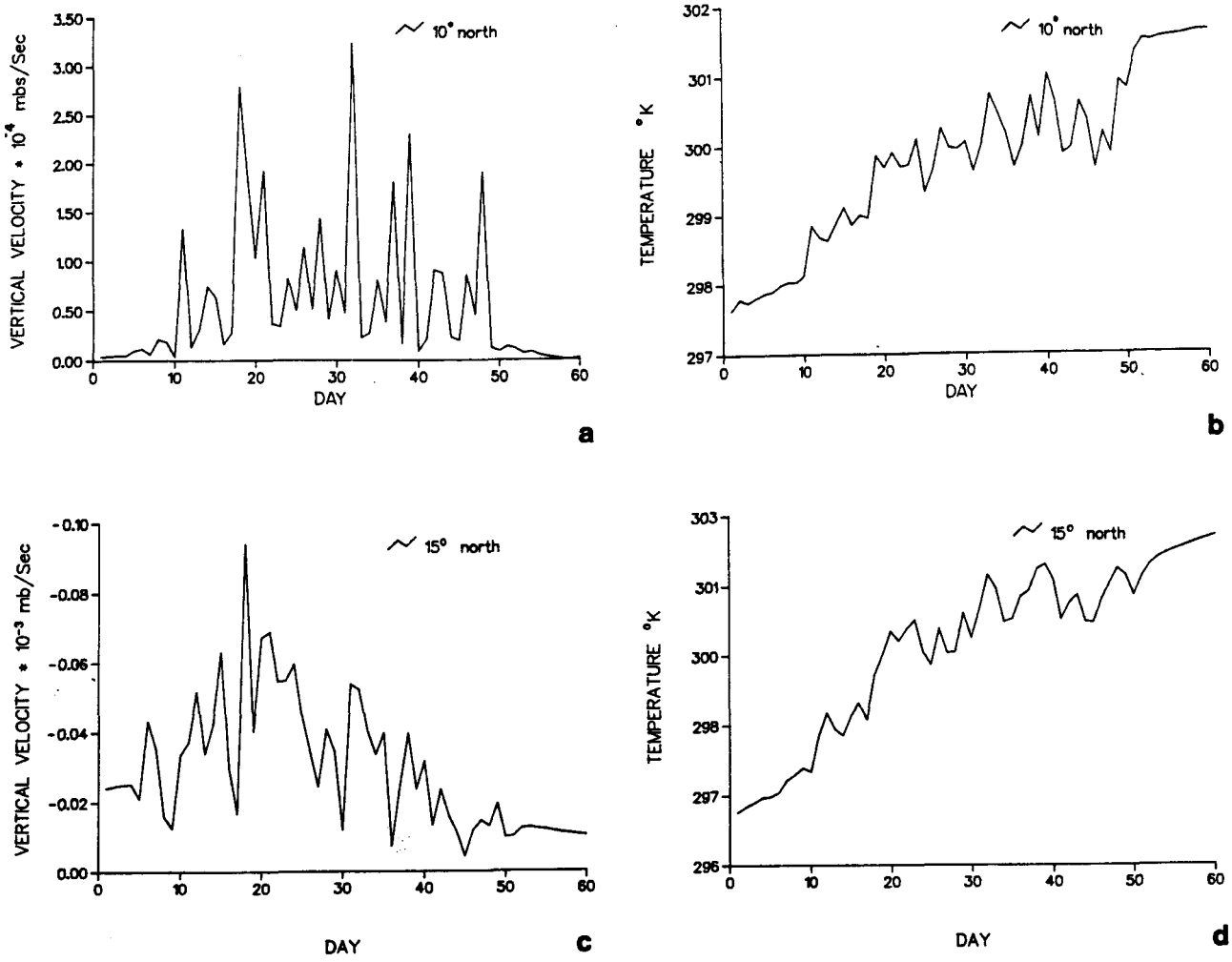

Fig. 19 a, b and c, d. Time history of vertical velocity (at 900 mb) and surface potential temperature at 10° and 15° N respectively beginning with spring equinox of the 20th year integration (LOP). Quasi-periodic oscillations with periods of 8 to 15 days can be seen

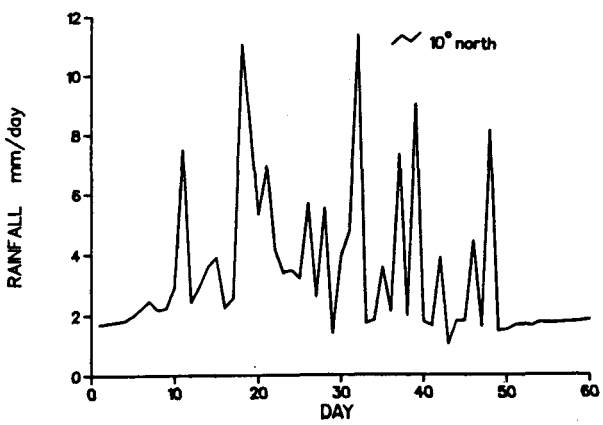

Fig. 19 e. Same as in Fig. 19 but for rainfall at 10° N

at 10° N and by day 20 there is a decrease in the temperature at 10° N with relatively higher temperatures at 5° and 15° N. By day 26 the surface temperature maximum is at 20° N. This shows a clear poleward propagation of the surface temperature peak. Though the amplitude of the oscillation in the sensible heat flux is small, propagation of peak can also be seen. Poleward propagation of peaks with time of all components is seen in these figures.

On day 11 at 10° N, vertical velocity, latent heat flux and surface temperature peaks are in phase while by day 20 vertical velocity and surface potential temperature peaks propagate poleward with the latent heat flux lagging behind them. By day 23 vertical velocity and surface temperature

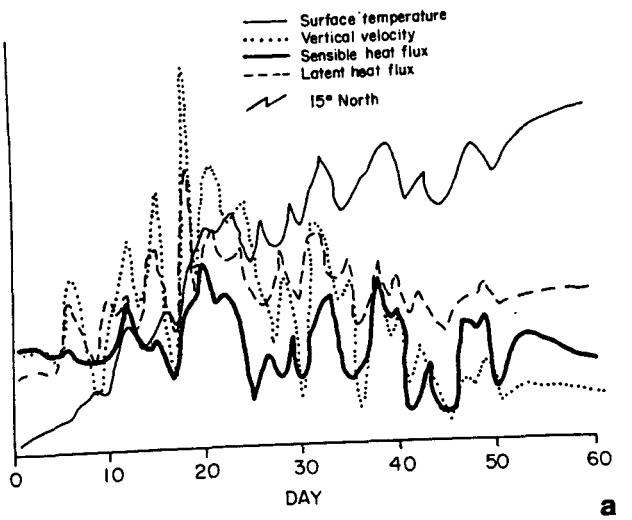

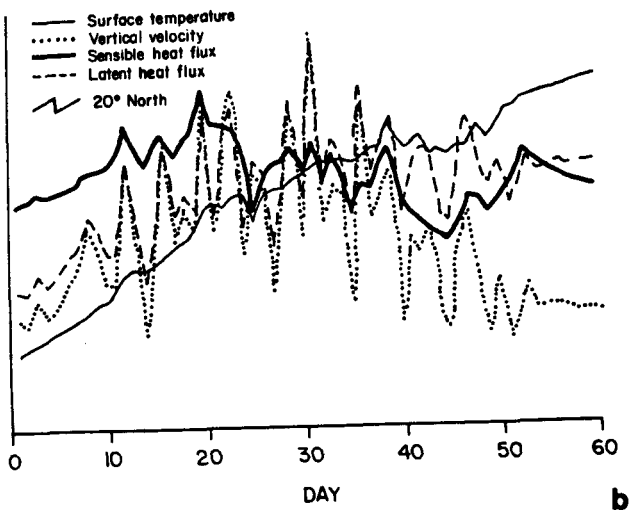

Fig. 20a, b. Time history of vertical velocity (at 900 mb), latent heat flux, surface potential temperature and sensible heat flux at 15° and 20° N respectively beginning with spring equinox of the 20th year of integration. Vertical velocity and latent heat flux peaks lag behind surface potential temperature peaks

maxima are over 20° N and the amplitude of the peak of the latent heat flux increases considerably over this zone. By day 23 the peaks are in phase at 5° N and 20° N. The sensible heat flux also shows an increasing trend with latitude and oscillations are evident in Fig. 21 (d). Webster (1983) using a primitive equation model showed that a perturbation in the sensible heat flux can lead to the perturbation and poleward propagation of other parameters. It appears that in Webster's model sensible heat flux is the crucial component responsible for the poleward propagations of other variables. The maximum values of various parameters (latent heat flux, vertical velocity etc.,) in the present model are comparable (although smaller) to that of Webster (1983). The decrease in magnitude may be due to the missing advection terms in the momentum equations and implicit treatment of the dynamics in the present model. Also while evaluating the vertical velocity only geostrophic component was considered and the ageostrophic component was not included. Maximum values of various components in the present model at 10° N are 4.76×10^{-6} °K/sec for latent heating rate, 0.44×10^{-6} °K/sec for sensible heating rate and 1.1×10^{-4} mb/sec for vertical velocity which are smaller magnitudes as compared to the results of Webster (1983).

It follows that in the present model a positive perturbation and its poleward propagation of the surface temperature can lead to the perturbation and poleward propagation of other components. It is encouraging to find that a simple energy balance model could simulate the northward progression of quasi-periodic oscillations during the pre- and post-monsoon periods in the tropical region.

Behavior of the ITCZ over an unbounded ocean may not be similar to that over a bounded ocean where fluid motions are subject to continental influences (Pike, 1972). In the global ocean (WO-OP) case of the present model, the ITCZ migration is confined to 5° latitude only. But in the LOP case, ITCZ over the ocean shifts further South to a latitude of 10° (Fig. 17). This shows the effect of continent on the oceanic ITCZ location.

Vertical velocity patterns for the land-ocean planet (LOP) domain for the 18th to 20th years of time integration are shown in Fig. 22. Even though there are small changes in the relative magnitudes with years, the onset and withdrawal of the model's monsoon are similar every year with essentially the same features.

5. Conclusions

A zonally averaged energy balance model with feedback mechanisms was constructed to simulate the poleward limits of the ITCZ using different

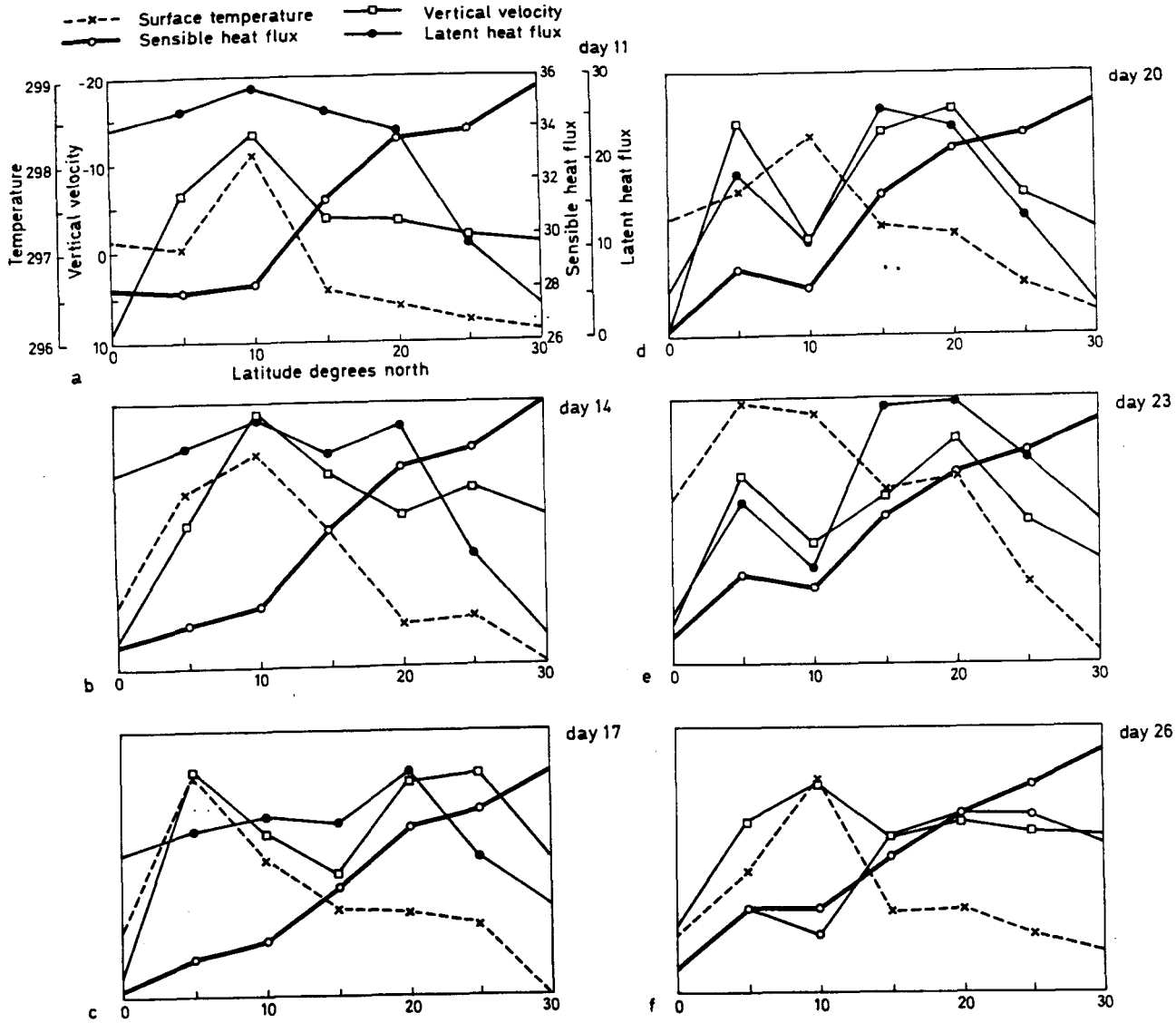

Fig. 21 a thru f. Latitudinal distribution of vertical velocity at 900 mb (Units: 10^{-5} mb/sec), Latent heat flux (10^{1} W/m^2), surface potential temperature (°K) and sensible heat flux (W/m^2) respectively for the days 11, 14, 17, 20, 23, and 26 starting from the spring equinox of the 20th year integration (LOP). Poleward propagation of various parameters can be seen

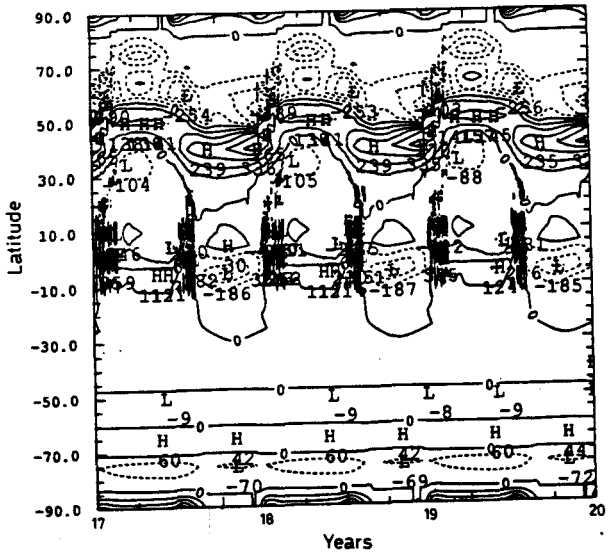

Fig. 22. Time Latitude section of vertical velocity (at 900 mb) for years 18, 19 and 20 beginning with the spring equinox for LOP case. Scale: 10^{-6} mb. Contour interval: 60×10^{-6} mb. Dashed contours represent negative values. Models's monsoon repeats with similar features

lower boundary conditions and to study a simple monsoon system as a result of differential heating between the continent and the ocean. The results show that the ITCZ migrates to a greater extent over the continents (up to 25° north and south) than over the oceans. Migration over the ocean is confined to 10° north and south. These results are in good agreement with the observed poleward limits of the ITCZ. The "events", which are prominent features during the monsoon season, appear only in the LOP (Land-Ocean-covered Planet) domain where hydrological processes and differential heating due to land-ocean contrasts exist. These "events" are absent in the OP (Ocean Planet) and the LP (Land Planet) domains. Periods of the oscillations are about 8 – 15 days and are prominent only during the onset and withdrawal of the model's monsoon. Northward propagation of the surface temperature perturbation appears to cause changes in sensible heat flux which in turn causes perturbations in vertical velocity and latent heat flux fields. The time of onset (April) and the withdrawal (October) of the model's monsoon is in good agreement with the observed time periods. During the months of June, July and August the propagation of the "events" disappears leaving a uniform distribution of various fields. But the observations indicate that during monsoon season the propagation of the events with varying periodicities appear to be a continuous feature (Sikka and Gadgil, 1980). The temporary absence of the "events" in the model results may be due to the implicit treatment of the model dynamics and absence of nonlinear terms in the momentum equations. Moreover, the parameterizations used for solving the components of the surface wind field (Sellers, 1973) in a way fixes the geographical location of the Ferrel Cell. The present model results may not be applicable to the real atmosphere in which many complex processes interact nonlinearly and the realistic representation may require a General Circulation Model. But the present model, like other climate models, necessarily contains the parameterization of the integrated effects and simulates some of the observed features of ITCZ and explains the basic mechanism responsible for the northward progression of the "events".

Acknowledgement

The authors are thankful to Dr. Sankar-Rao, Indian Institute of Science, Bangalore, India, for many helpful suggestions. Also the authors are thankful to the reviewers for their valuable comments. This work was partially supported by the Naval Research Laboratory, Washington, D.C. and by the Division of International Programs, National Science Foundation under the Grant INT-82-19710.

References

Chang, C.-P., 1986: Kelvin wave-CISK: a possible mechanism for the 30 – 50 day oscillations. International conference on Monsoon and Mesoscale Meteorology, Taipai, 1986, 236–245.

Estoque, M. A., Douglas, M., 1978: Structure of inter tropical convergence zone over GATE area. *Tellus*, **30**, 55–61.

Fritz, S., 1960: Dynamics of climate, Pfeftor, R.L., Ed. New York, Pergamon press, 96–100.

Godbole, R. V., 1973: Numerical simulation of the Indian Summer monsoon. *Indian J. Meteor. Geophys.*, **24**, 1–14.

Goswami, B. N., Shukla, J., 1984: Quasi-periodic oscillations in a symmetric general circulation model. *J. Atmos. Sci.*, **41**, 20–37.

Goswami, B. N., Shukla, J., Schneider, E. K., Sud, Y. C., 1984: Study of the dynamics of the inter tropical convergence Zone with a symmetric version of the GLAS climate Model. *J. Atmos. Sci.*, **40**, 1584–1591.

Hann, D. G., Manabe, S., 1975: The role of the mountains in the South-Asian monsoon circulation. *J. Atmos. Sci.*, **32**, 1515–1541.

Hubert, L. J., Krueger, A. F., Winston, J. S., 1969: The double inter tropical convergence Zone – Fact or Fiction? *J. Atmos. Sci.*, **37**, 515–533.

Kondratyev, K. Yao., 1969: *Radiation in the Atmosphere.* New York: Academic press.

Krishnamurti, T. N., Bhalme, H. H., 1976: Oscillation of a monsoon system, Part I: Observational aspects. *J. Atmos. Sci.*, **33**, 1937–1954.

Krishnamurti, T. N., 1986: Analysis of the 30 – 50 day oscillation from several years of observations. International conference on monsoon and mesoscale meteorology, Taipai, 1986, 246–257

Kurihara, Y., 1971: Seasonal variation of temperature in an atmosphere at rest. *J. Meteor. Soc. Japan*, **49**, 537–544.

Lau, N. C., Lau, K. M., 1986: The structure and propagation of Intraseasonal oscillations appearing in a GFDL General Circulation Model. *J. Atmos. Sci.*, **43**, 2023–2047.

Murakami, T., Godbole, R. V., Kelkar, R. R., 1968: Numerical experiment of the monsoon along 80 E longitude. Sci Rep. No. 62, Indian Meteorological Department, Poona, 51 pp.

Murakami, T., 1977: Spectrum analysis relevant to Indian monsoon. *Pure Appl. Geo phys.*, **115**, 1149–1166.

Pike, A. C., 1971: Inter tropical convergence zone studied with an interacting atmosphere and ocean model. *Mon. Wea. Rev.*, **99**, 469–477.

Pike, A. C., 1972: Response of a tropical atmosphere and ocean model to seasonally variable forcing. *Mon. Wea. Rev.*, **100**, 424–433.

Pushitov, P. Yu., Gutman, L. N., 1970: A baroclinic model of the atmospheric zonal circulation in the equatorial region. Academy of Sciences, Institute of Atmospheric Physics, USSR.

Rao, Y. P., 1976: Southwest Monsoon. Meteorological Monograph, Synoptic meteorology, India Meteorological Department, No. 1/76.

Reginald, E. N., John, W. K., Dayton, G. V., George, J. B., 1974: *The General Circulation of the Tropical Atmosphere and Interactions with Extra Tropical Latitudes*. Vol. 1 and 2, The Massachusetts Institute of Technology, 862 pp.

Riehl, H., 1979: *Climate and Weather in the Tropics*. New York: Academic Press, 661 pp.

Saltzman, B., Vernekar, A. D., 1971: An equilibrium solution for the axially symmetric component of the earth's macro climate. *J. Geophy Res.*, **76**, 1498–1524.

Sellers, W. D., 1965: *Physical Climatology*. University of Chicago Press, 587 pp.

Sellers, W. D., 1973: A global climate model based on the energy balance of the earth-atmosphere system. *J. Appl. Meteor.*, **8**, 392–400.

Sikka, D. R., Gadgil, S., 1980: On the maximum cloud zone and the ITCZ over Indian longitudes during the South West monsoon. *Mon. Wea. Rev.*, **108**, 1840–1853.

Smith, W. L., 1966: Note on the relationship between total precipitable water and surface dew point. *J. Appl. Meteor.*, **5**, 726–727.

Webster, P. J., Chou, L. C., 1979 a: Low frequency transitions of a simple monsoon system. *J. Atmos. Sci.*, **37**, 368–382.

Webster, P. J., Chou, L. C., 1979 b: Seasonal structure of a simple Monsoon system. *J. Atmos. Sci.*, **37**, 354–367.

Yasunari, T., 1979: Cloudiness fluctuations associated with the Northern Hemisphere summer monsoon. *J. Meteor. Soc. Japan*, **57**, 227–262.

Authors' addresses: Kirankumar Alapati and Sethu Raman, Department of Marine, Earth and Atmospheric Sciences, North Carolina State University, Raleigh, NC 27695-8208, U.S.A.

Printed in Austria